Korea-Australia Rheology Journal
Vol. 16, No. 2, June 2004 pp. 101-108

Asymmetric flows of non-Newtonian fluids in symmetric stenosed artery

Hun Jung*, Jong Wook Choi[1] and Chan Guk Park[2]

Graduate School, Department of Mechanical Engineering, Chonnam National University, Kwangju 500-757, Korea
[1]School of Mechanical and Automotive Engineering, Sunchon National University, Sunchon 540-742, Korea
[2]Department of Mechanical Engineering, Chonnam National University, Kwangju 500-757, Korea

(Received November 26, 2003; final revision received May 31, 2004)

Abstract

The hemodynamics behavior of the blood flow is influenced by the presence of the arterial stenosis. If the stenosis is present in an artery, normal blood flow is disturbed. In the present study, the characteristics of pulsatile flow in the blood vessel with stenosis are investigated by the finite volume method. For the validation of numerical model, the computation results are compared with the experimental ones of Ojha *et al.* in the case of 45% stenosis with a trapezoidal profile. Comparisons between the measured and the computed velocity profiles are favorable to our solutions. Finally, the effects of stenosis severity and wall shear stress are discussed in the present computational analysis. It can be seen, where the non-dimensional peak velocity is displayed for all the stenosis models at a given severity of stenosis, that it is exponentially increased. Although the stenosis and the boundary conditions are all symmetric, the asymmetric flow can be detected in the more than 57% stenosis. The instability by a three-dimensional symmetry-breaking leads to the asymmetric separation and the intense swirling motion downstream of the stenosis.

Keywords : stenosis, wall shear stress, non-Newtonian fluid, numerical analysis, physiological flow, instability flow

1. Introduction

The intimal thickening of stenotic artery was understood as an early process in the beginning of atherosclerosis. Atherosclerosis is the leading cause of death in many countries. There is considerable evidence that vascular fluid dynamics plays an important role in the development and progression of arterial stenosis, which is one of the most widespread diseases in human beings. The fluid mechanical study of blood flow in artery bears some important aspects due to the engineering interest as well as the feasible medical applications. The hemodynamic behavior of the blood flow is influenced by the presence of the arterial stenosis. If the stenosis is present in an artery, normal blood flow is disturbed. The study of pulsatile flow through a stenosis is motivated by the need to obtain a better understanding of the impact of flow phenomena on atherosclerosis and stroke. In order to understand the effect of stenosis on blood flow through and beyond the narrowed segment of the artery, many studies have been undertaken experimentally and theoretically.

Although a large number of investigations have led to better understanding of the flow disturbances induced by a stenosis, most of the theoretical and experimental studies have been performed under the simplifying assumptions. Many theoretical analyses have been assumed in the steady state (Forrest and Young, 1970 etc.). Forrest and Yong (1970) reported experimentally that there is a considerable difference between the blood flow and the water one through a stenosed tube and that the effect of the non-Newtonian property of blood should not be neglected. The detailed velocity profiles were obtained for the pulsatile flow through tubes with the constrictions of different symmetry and the degrees of blockage using the photochromic tracer methods (Ojha *et al.*, 1989). The post-stenotic velocity flow field corresponding to oscillatory, pulsatile and physiological flow waveforms was studied using a pulsed Doppler ultrasonic velocimeter (Deplano, V. and M. Siouffi, 1999). From their observations, it has observed that the velocity field is highly dependent on the flow waveform, particularly downstream from stenosis. Also, the strong flow reversal and recirculation were found to be uniformly distributed around the circumference of the walls in the downstream of stenosis.

Some experiments have shown that the maximum Reynolds number which can sustain the axisymmetric flow is about 500 for stenosis (Khalifa *et al.*, 1981; Solzbach *et al.*, 1987). Khalifa and Giddens conducted experiments aiming at relating the level of disturbances of the poststenotic flow

*Corresponding author: jmbj0728@nate.com

to the degree of stenotic obstruction (1981). Saad demonstrated that the flow disturbances are a sensitive indicator of mild to moderate stenoses (1998). However, the flow through a stenosis is far from being well understood. The aforementioned experimental studies have demonstrated that the stenotic pulsatile flow exhibits the disturbance phenomena of flow which deviate the flow from the laminar behaviour. If the Reynolds number or the severity of stenosis becomes large, the flow through the stenosed blood vessels cannot be axisymmetric.

Numerical solutions of pulsatile flow have been reported by several investigators (John M Siegel *et al.*, 1996; Santabrata *et al.*, 2000 etc.), which has been done assuming the blood as a Newtonian fluid. Also, a number of researchers (Nakamura *et al.*, 1988; Nagatomo *et al.*, 1991 etc.) have studied the flow fields in consideration of the non-Newtonian property of blood. However, they did not study the effect of pulsation on the flow. A number of researchers have studied the flow of non-Newtonian fluids with the pulsation through arterial stenosis (Takuji *et al.*, 1998 etc.). However, the flow fields are limited to mild stenosis under the severity of 50%.

To our knowledge, a computational study of three dimensional, pulsatile and unstable flows through a stenosis has not previously been conducted. In the present study, the unsteady generalized Navier-Stokes equations are solved by a finite volume method. The pulsatile blood flow through a severe stenosed tube is analyzed numerically using a Carreau viscosity model as the constitutive equation of blood. The effects of the instability are examined on the wall shear stress and velocity.

2. Equations for simulations

2.1 Governing equations

It is well known that the blood behaves as a non-Newtonian fluid under a certain flow condition (Fung, 1984). The governing equations for the conservation of mass and momentum of an incompressible and non-Newtonian fluid are shown in the equations (1)-(2) which are the three dimensional, time-dependent Navier-Stokes equations.

$$\frac{\partial u_i}{\partial x_i} = 0 \tag{1}$$

$$\rho\left(\frac{\partial u_i}{\partial t} + u_j\frac{\partial u_i}{\partial x_j}\right) = -\frac{\partial p}{\partial x_i} + \frac{\partial \tau_{ij}}{\partial x_j} \tag{2}$$

The shear stress tensor is defined by the constitutive equation (3)

$$\tau_{ij} = \eta\left(\frac{\partial u_i}{\partial x_j} + \frac{\partial u_j}{\partial x_i}\right) \quad i, j = 1, 2, 3 \tag{3}$$

Obtaining the viscosity from measurements is a separate problem. In the steady conditions, the apparent viscosity was measured with a capillary viscometer Ubhellode. There are various models to describe the non-Newtonian behavior of the blood: Casson model(Shu Chien, 1975), Simpler model(Quemada, 1977). The complex rheological behavior of blood is approximated using a shear-thinning model by the Carreau model, where the apparent viscosity is expressed as a function of the shear rate as shown in the equation (4).

$$\eta = \eta_\infty + (\eta_0 - \eta_\infty)[1 + (\lambda \times \dot{\gamma})^2]^{\left(\frac{q-1}{2}\right)} \tag{4}$$

For $\dot{\gamma}$, a scalar measure of the rate of deformation tensor is the equation (5).

$$\dot{\gamma} = \sqrt{\frac{1}{2}\sum_i\sum_j \dot{\gamma}_{ij}\dot{\gamma}_{ji}} \tag{5}$$

The Carreau model is fitted to the experimental data, resulting in the following set of parameters:

$$\eta_0 = 0.056\ Pa \cdot s,\ \eta_0 = 0.00345\ Pa \cdot s,\ \lambda = 3.31s,\ q = 0.357 \tag{6}$$

The values of these parameters, obtained by fitting the data, are given in the caption of Fig. 1.

2.2. Solution procedure

The discretized forms of the transformed equations are obtained by a control volume formulation in a staggered grid. Each equation is integrated over its proper control volume and values of the dependent variable and its derivative at control surfaces are approximated in terms of nodal values at surrounding points. The resulting equations are solved using the SIMPLER (Semi-Implicit Method for Pressure-Linked Equations Revised) algorithm of Patankar (1980), formulated for use in the $(\xi - \eta)$ plane. Solutions are obtained iteratively, considering the following criterion convergence at each time step:

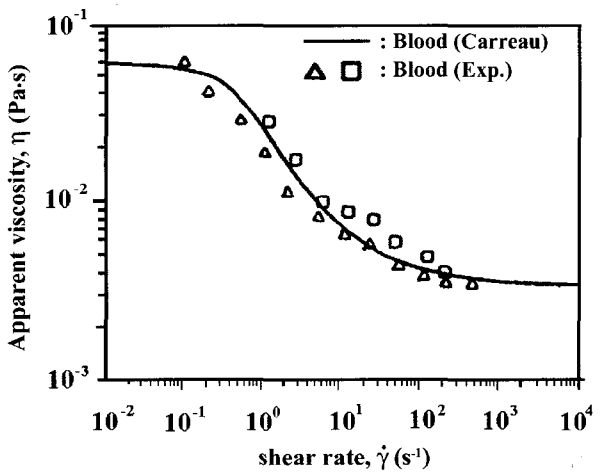

Fig. 1. Blood viscosity versus shear rate.

$\sum|\text{inflow}-\text{outflow}|<5\times10^{-4}$,

where the summation is over all control volumes. Numerical calculations are performed according to the following steps:

1. A first approximation for the u, v, w and p distribution is assumed.
2. Pressure equation is solved.
3. Equations are solved.
4. Equation is solved and u, v and w are corrected.
5. Steps 2 – 4 are repeated until the convergence criterion is satisfied.
6. The above calculations are repeated at each time step for several periods and the results obtained for each period are compared to those for the previous period. A periodic solution is obtained when the variables calculated at different points and at different times over two successive periods become almost identical.

3. Numerical model

3.1. Numerical validation

As the first step in our analysis, the numerical results are compared with the several experimental and analytic solutions with comparable transient laminar flow fields in straight or constricted. Here, the numerical results are compared with the experiment of Ojha *et al.* (1989) about velocity profiles of post-stenotic regions. As shown in Fig. 2, the geometry used in the validation is a 45% stenosis with a trapezoidal profile. The normalized distance form the centre of stenosis is given by $Z=Z'/D$. The pulsatile flow has waveform of 4.3 ± 2.6 m*l* with a period of 345 ms. The fluid has a density of 755 kg/m^3 and a viscosity of 0.00143 N/m^2 as deodorized kerosene (Shell-Sol 715). The Reynolds number is defined based on the blood vessel inlet diameter, the time-averaged mean velocity and a limiting high shear rate Newtonian viscosity, $Re=\rho UD/\mu_\infty$. This particular input pulse allows a direct change to the Womersley number, $Wo=r_0(2\pi/\nu T)^{1/2}$, the ratio of transient inertial effects to viscous effects, without altering the Reynolds number. The inlet pulse is a sinusoidal pulse with a mean Reynolds number of 575, and the maximum and minimum Reynolds numbers are 930 and 230, respectively. The Womersley number for this pulse was 7.5.

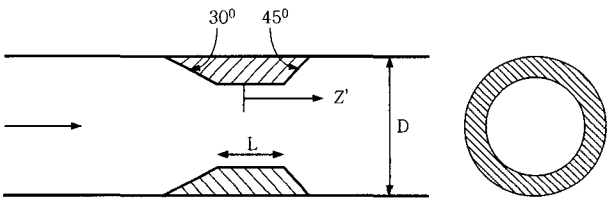

Fig. 2. The geometry of 45% axisymmetric stenosis used in the simulation, where $L=1.5$ mm and $D=5.0$ mm.

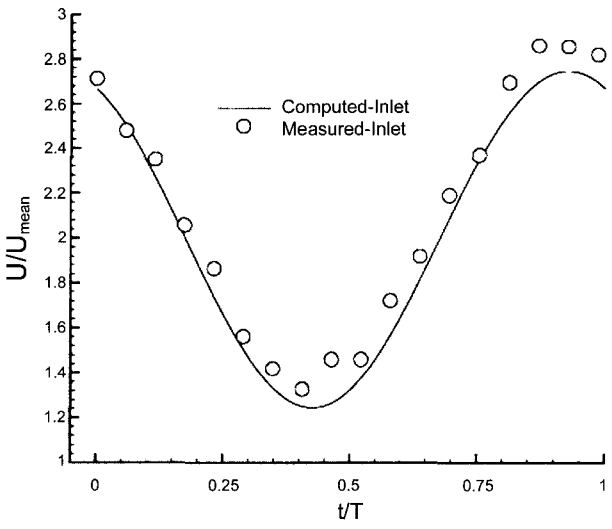

Fig. 3. Inlet centerline velocity profile.

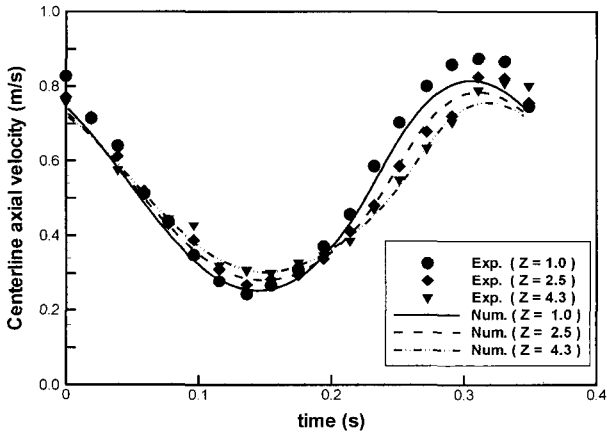

Fig. 4. Comparison of centerline axial velocity between predictions and measurement.

To analyze velocity variations of post-stenotic region, the input centerline variations versus time are compared in the Fig. 3. The inlet boundary condition is presumed by fully developed axial velocity profiles calculated from the time-dependent velocity. As can be seen, the inlet centerline velocities are similar throughout the pulse, except near the zenith of the pulse. This additional acceleration in the experimental input pulse causes slight discrepancies with the data. Comparison between the measured and computed velocity profiles are shown in Fig. 4. The differences between the predictions and experimental data are found to be great near the zenith of the pulse as has been pointed out. However, it is seen that the agreement is generally good.

3.2. Physical model

The blood vessel geometry is determined by the radius r_0 and the local, smooth axisymmetric constriction as shown in the equation (7).

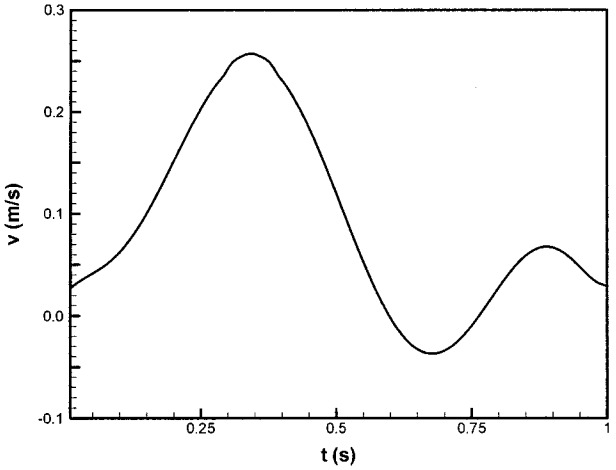

Fig. 5. Physiological velocity profile used in the pulsatile simulation.

$$r(z) = \begin{cases} r_0 - \frac{\delta}{2}\left[1+\cos\left(\frac{\pi z_0}{l}\right)\right] & \text{if } |z|<1 \\ r_0 & \text{otherwise} \end{cases} \quad (7)$$

Where δ is the constricted radius (radius in the narrowest part, the neck); r_0 is unconstricted radius. The origin $z = 0$ corresponds to the neck of the stenosis. The axial coordinate z is normalized by the blood vessel diameter; z_0 is the stenosis half-length. l is fixed at the large value of $2r_0$ in this research, so that stenosis has a considerable influence on flow.

Stenosis severity is commonly defined as the equation (8).

$$s = (d - \delta)/d \times 100\% \quad (8)$$

In order to mimic physiological flow conditions, a pulse velocity is used with time-varying function similar to the one used by Siouffi *et al.* (1984). The period of the heart beat is supposed to be 1s. The tubular model with a local constriction and flow input profile are shown in Fig. 5 and Fig. 6. The several numerical analyses have been conducted using different blood vessel lengths upstream and downstream of the stenosis in order to ensure independence of the results from the position of the inflow and outflow boundaries. We have found that 25D and 60D lengths upstream and downstream, respectively, are sufficient. Also, it were carried out on a grid containing $27 \times 27 \times 150$ grid points, which was confirmed to not influence the numerical results very much.

The boundary conditions are the following. We are not concerned with the moving boundary wall. On the rigid no-slip wall, the velocity at the wall is vanished. At the inflow section, the radial velocity vanishes while the axial component is calculated on the basis of the flow rate and the type of fluid. At the inlet, the main flow is assumed to be fully developed. At the outflow section, the second-order

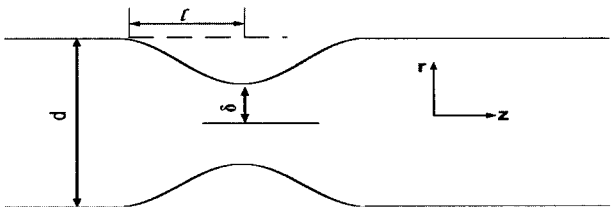

(a) Geometry of constricted blood vessel

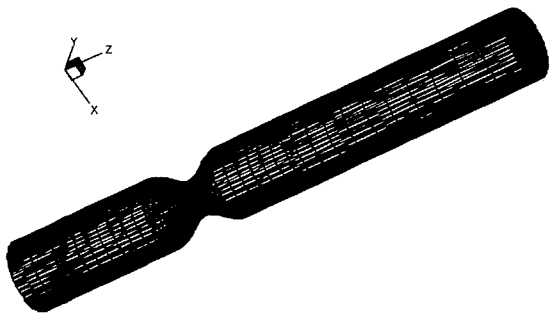

(b) Finite volume mesh

Fig. 6. Geometry of the stenosed arterial segment.

derivatives of the flow variables were set equal to zero.

4. Results and discussion

To study the influence of stenoses on the flow, the computations were conducted for various values of the parameters on the severity of stenoses s. In our numerical computation, those were conducted for stenoses with severities from 50% to 75% to perform a careful parameter analysis. The stenoses with severities less than 50% are considered mild for carotid arteries. The instantaneous streamlines are shown during a cycle of pulsatile flow at intervals of 0.125s for the case of 50%, 57% and 75% in Fig. 7 ~ 9. The non-dimensional Womersley number that measured the frequency of the pulsation was found to be 6.95.

For the case of 50% stenosis, the streamline distribution inside blood vessel at each time step is shown in Fig. 7. At $t = 0.125$, the small vortex is formed near the wall distal to the stenosis of the blood vessel. As time goes on, the size of the vortex grows larger. The fluid flow at inlet is decelerated after $t = 0.375$, the vortex formed on early nearly disappears. At $t = 0.375$, as the inlet velocity decreases, recirculation at the post-stenosed part of the blood vessel increases. When the velocity reaches its negative value at $t = 0.625$ and fell low the average velocity, the recirculation (both downstream and upstream) are swept off the wall. At $t = 0.75$, where the flow reverses direction is further shown in Fig. 7, large recirculation zones occupy both distal and proximal region to the stenosis. At $t = 0.875$, as the velocity accelerates again during diastole, this upstream and downstream recirculation disappears.

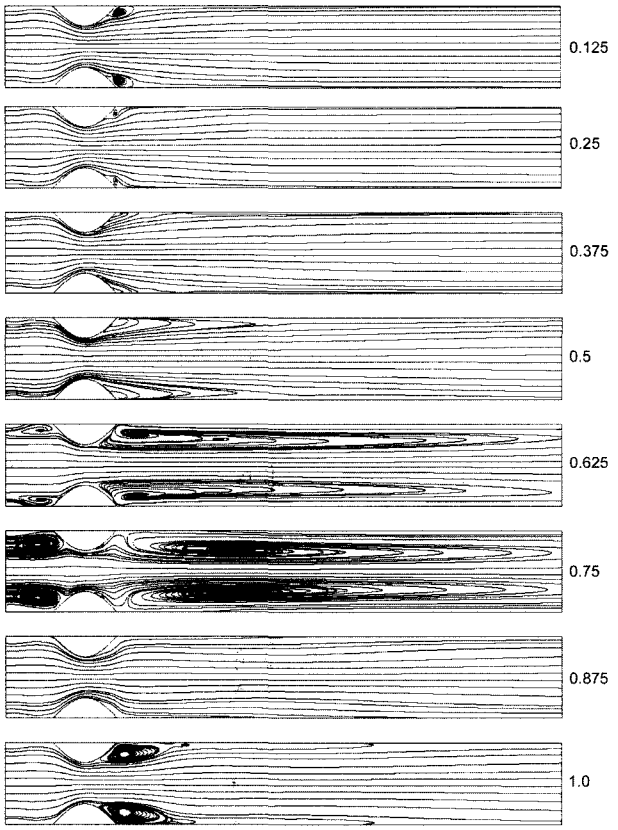

Fig. 7. Instantaneous streamline patterns at different temporal points in the pulsatile flow, 50% of stenosis.

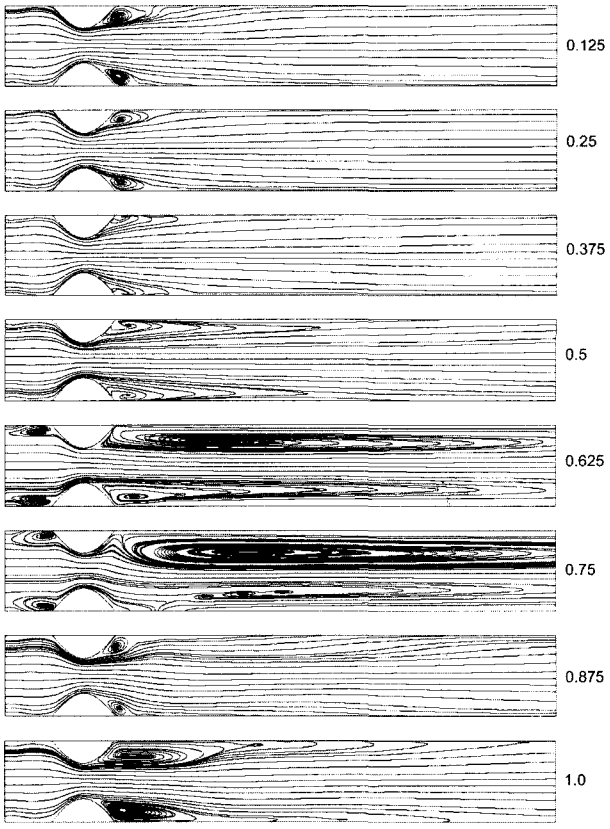

Fig. 8. Instantaneous streamline patterns at different temporal points in the pulsatile flow, 57% of stenosis.

Fig. 8 shows considerable variation of the flow pattern through one cycle of the 57% stenosis. Comparing streamlines of the 50% stenosis with those of the 57% stenosis, the separated region and the strength of the vortex are very different in the recirculation zone. Although the stenosis and the boundary conditions were all axisymmetric, it can be detected asymmetric flow in the separated flow region downstream of the stenosis. The jet flow went to one side of the tube and there was a big flow separation region distal to stenosis. This is manifested by a breaking of the flow symmetry similar to the symmetry-breaking bifurcation occurring in two-dimensional, suddenly-expanded flow (D. Drikakis, 1997).

We also have plotted those of 75% stenosis in the Fig. 9. If it becomes the 75% stenosis, the flow in the downstream region is more complicated motions and takes place of vortex shedding. This flow instability through a stenosis has been discussed several previous experimental (Chedron *et al.*, 1978; Fearn *et al.*, 1990) and computational (D. Tang *et al.*, 1999; F. Mallinger *et al.*, 2002) works.

In Fig. 10, asymmetric flow pattern in different cross-sections downstream of the stenosis are shown by means of isocontour plots of the streamwise velocity. The breaking of the flow symmetry is associated with the formation of a vortex on the upper and lower walls. The instability is manifested by a symmetry breaking of the flow separation. As the flow is further downstream, the vortices emerge from the near-wall region and gradually occupy a large part of the cross-sectional area. In the present case, the breaking of the flow axisymmetry is associated with changes in both the longitudinal and circumferential direction, but the intensity of asymmetries in the secondary plane readily decreases further downstream. The asymmetric flow behavior persists over a few radii downstream prior to the flow becoming fully axisymmetric again.

If this physiological phenomenon happens, the arterial diseases of stenosis or atherosclerosis become worse and the serious damage to the vessel wall may occur. Also, this closed recirculation zone, with low and high shearing stresses, can be the origin of red cell damage and thrombosis formation. The stenosis will progress further and consequently artificial arterial segment should be replaced. It can also be seen from Fig. 11, where the non-dimensional peak velocity is displayed for all the stenosis models at a given severity of stenosis.

This shows that the more severity of stenosis increases, the more the velocity of flow increases. It is showed that the non-dimensional peak velocity amount to about triple of averaged velocity at the 57% stenosis. It is seriously increased after 57% stenosis, and we can see that asym-

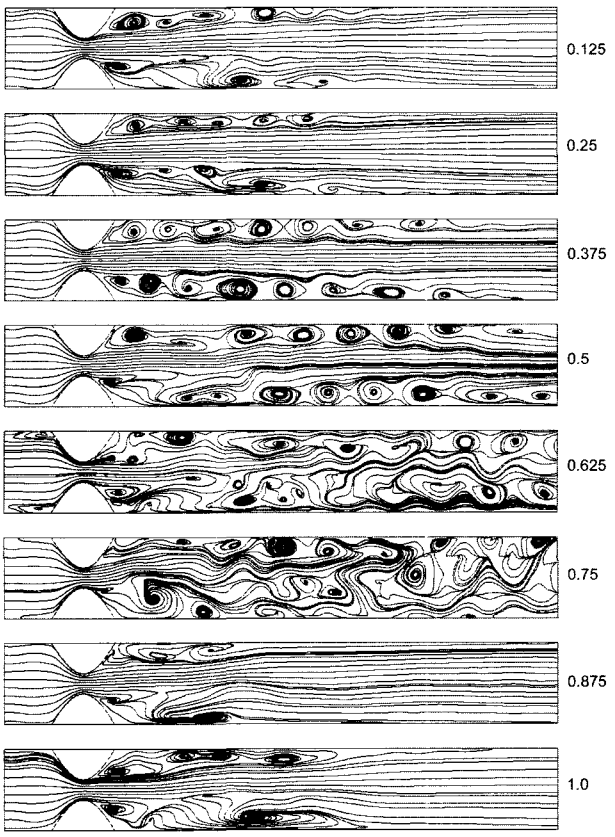

Fig. 9. Instantaneous streamline patterns at different temporal points in the pulsatile flow, 75% of stenosis

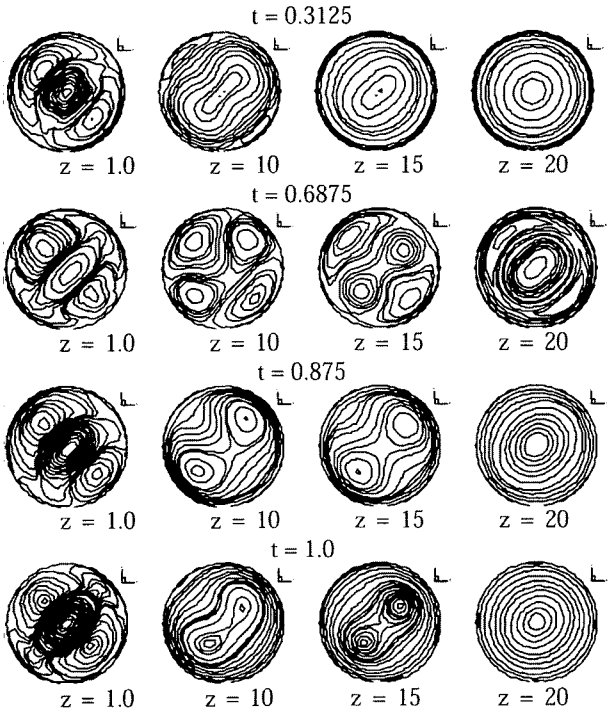

Fig. 10. Isocoutours of the streamwise velocity at different time instants and cross-sections.

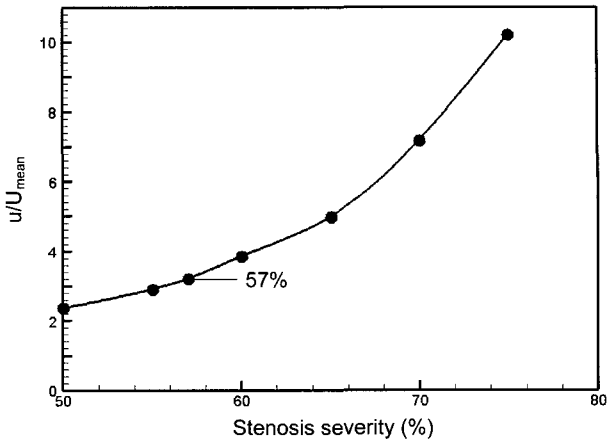

Fig. 11. Non-dimensional velocity according to Stenosis severity of Blood.

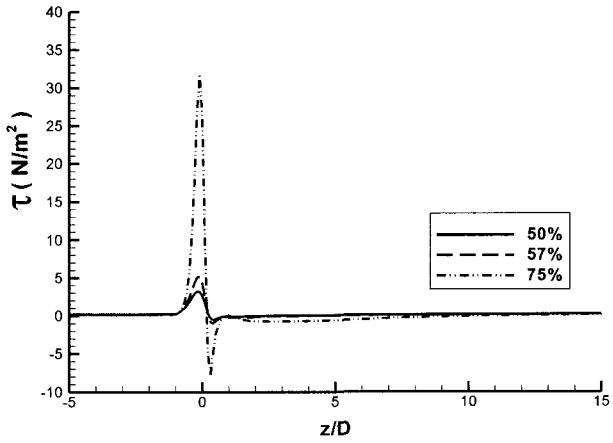

Fig. 12. Plot of shear stress along blood vessel wall.

metric flow is more complicated. The severity of the stenosis has a significant effect on the general features such as the separation Reynolds number and the size of the separation region, while the shape of the stenosis has less effect. Also, high velocity causes high shear stress at the blood vessel wall which may be related to platelet activation and plaque cap rupture (Tang *et al.*, 1999).

When a vulnerable lesion is subjected to triggering events over a sufficiently long time and of a sufficient magnitude that the structural integrity of the plaque is compromised, the plaque rupture or the fracture may occur. A vulnerable atherosclerotic plaque contains a large necrotic core, and is covered by a thin fibrous cap. Triggering events are believed to be primarily hemodynamic, including cap tension, compression, bending, or torsion of the artery (Tang *et al.*, 1999; Stroud *et al.*, 2000).

The distributions of time averaged wall shear stress (WSS) about severity condition of stenosis is shown in Fig. 12. The peak values of WSS are exerted at the stenosed part of the vessel and negative wall shear stress are seen where a vortex exists. The flow with the 75% stenosis is

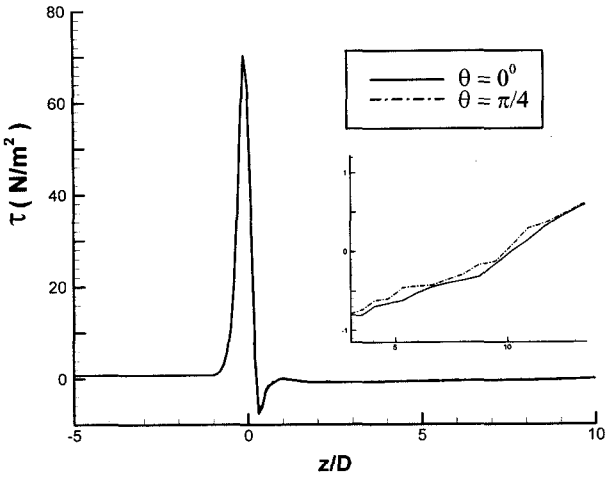

Fig. 13. Wall shear stress at two different angular positions in the 75% stenosis.

dominated by the effect of wall shear stress regardless of acceleration or deceleration, especially at the stenosis position.

Fig. 13 presents the maximum wall shear stress along two lines $\theta = 0°$, $\pi/4$ with the 75% stenosis. Maximum shear stress appeared at the throat of the stenosis as expected. The maximum shear stress along the 0° line is similar to the maximum along the $\pi/4$ line.

4. Conclusions

In the present study, the numerical results are obtained for the physiological phenomena of the blood flow. Three dimensional numerical simulations of pulsatile flow through a symmetric stenosis revealed the existence of instability solutions. Analysis of the velocity and wall shear stress has shown that the most significant flow changes can be grouped into poststenotic regions. The high stress is exerted near the stenosed point of the blood vessel due to the fast flow and the serious physical damage may occur due to the stress. It can also be seen, where the non-dimensional peak velocity is displayed for all the stenosis models at a given severity of stenosis, that it is exponentially increased. As the increase of stenosis severity, the blood vessel with stenosis and the boundary conditions were symmetric, and the asymmetric flow is detected in the separated flow region downstream of the stenosis. The results demonstrate that the model is capable of predicting the hemodynamics features most interesting to physiologists. It can be used to predict fast stenotic flow patterns on an individual basis. It can also be used for studying other parametric effects.

Acknowledgements

This research was supported in part by a grant from Brain Korea (BK21) in 2001.

References

Chaturani, P. and R.P. Samy, 1985, A study of non-Newtonian aspects of blood flow through stenosed arteries and its applications in arterial disease, *Biorheology* **22**, 521-531.

Chaturani, P. and R.P. Samy, 1986, Pulsatile flow of Cassons fluid through stenosed arteries with applications to blood flow, *Biorheology* **23**, 499-511.

Chendron, W. and F. Durst *et al.*, 1978, Asymmetric flows and instabilities in symmetric ducts with sudden expansion, *J. Fluid Mech.* **84**, 13-31.

Drikakis, D., 1997, Study of bifurcation flow phenomena in incompressible sudden-expansion flows, *Phy. Fluids* **9**, 76-87.

Fearn, R.M. and T. Mullin, 1990, Nonlinear flow phenomena in a symmetric sudden expansion, *J. Fluid Mech.* **211**, 595-608.

Forrest, J.H. and D.F. Young, 1970, Flow through a converging-diverging tube and its implications in occlusive vascular disease, *Journal of Biomechanics* **3**, 307-316.

Francois, M. and D. Dimitris, 2003, Instability in three-dimensional, unsteady, stenotic flows, *Int. J. Heat and Fluid Flow* **23**, 657-663.

Fung, Y.C., 1984, Biodynamics: Circulation. Springer, New York.

John, M. Siegel and C.P. Markou *et al.*, 1994, A scaling law for wall shear rate through an arterial stenosis, *Journal of Biomechanical Engineering Transactions ASME* **116**, 446-451.

Khalifa, A.M.A. and D.P. Giddens, 1981, Characterization and evolution of poststenotic flow disturbances, *J. Biomechanics* **14-5**, 279-296.

Lee, K.W. and X.Y. Xu, 2002, Modelling of flow and wall behaviour a mildly stenosed tube, *Med. Eng. & Phy.* **24**, 575-586.

Misra J.C. and M.K. Patra *et al.*, 1993, A non-Newtonian fluid model for blood flow through arteries under stenotic conditions, *Journal of Biomechanics* **26**, 1129-1141.

Nagatomo, M., B.R. Shin, T. Ikohangi and H. Daiguji, 1991, Proc. 5th CFD symp., 275-278.

Nakamura, M. and T. Sawada, 1988, Numerical study on the flow of a non-Newtonian fluid through an axisymmetric stonesis, *Journal of biomechanical Engineering* **110**, 137-143.

Nakamura, M. and T. Sawada 1990, Numerical study on the unsteady flow of non-Newtonian fluid, *Journal of biomechanical Engineering* **112**, 110-103

Ojha, M. and R.S.C. Cobbold *et al.*, 1989, Pulsatile flow through constricted tubes: an experimental investigation, *J. Fluid Mech.* **203**, 173-197.

Patankar, S.V., 1980, Numerical Heat Transfer and Fluid Flow, Hemisphere, Washington, DC.

Quemada, D., 1977, Rheology of concentrated disperse systems. III. General features of the proposed non-Newtonian model. Comparison with experimental data, *Rheol. Acta* **17**, 643.

Santabrata Chakravarty and Ashis Kr. Sannigrahi, 1998, An analytical estimate of the flow-field in a porous stenotic artery subject to body acceleration, *Internal Journal of Engineering Science* **36**, 1083-1102.

Shu Chien and S. Usami *et al.*, 1984, Blood flow in small tube, In American Physiology Society Handbook of Physiological,

Section, the cardiovascular system, **4**, Renkins, Bethesda, MD, 217-419.

Siouffi, M. and R., Farahifar, D. *et al.*, 1984, The effect of unsteadiness on the flow through stenoses and bifurcations, *J. Biomechanics*, **17**, 299-315.

Solzbach, U. and A. Zeiher *et al.*, 1987, Effect of stenotic geometry on flow behaviour across stenotic models, *J. Biomechanics* **25**, 543-550.

Stroud, J.S. and S.A. Berger *et al.*, 2000, Influence of stenosis morphology on flow through severely stenotic vessels: implications for plaque rupture, *J. Bio.* **33**, 443-435.

Takuji, I. and Luis F.R. Guimaraes *et al.*, 1998, Effect of non-Newtonian property of blood on flow through a stenosed tube, *F. Dyn. Res.* **22**, 251-264.

Tang, D., C. Yang, Y. Huang and D.N. Ku, 1999, Wall stress and strain analysis using a three-dimensional thick-wall model with fluid-structure interactions for blood flow in carotid arteries with stenoses, Computers and Structures **72**, 341-377.